International Journal of
Plasma Environmental Science and Technology

Regular Paper DOI: 10.34343/ijpest.2021.15.e02008

In situ transmission infrared spectroscopy of plasma-assisted CO_2 hydrogenation on ZnO: Role of catalyst support materials

Atsushi Saito[1,2], Zunrong Sheng[1], Dae-Yeong Kim[1], Yutaka Imamura[2], Tomohiro Nozaki[1,*]

[1] Department of Mechanical Engineering, Tokyo Institute of Technology, Tokyo 152-8550, Japan
[2] Innovative Technology Laboratories, AGC Inc., Yokohama 230-0045, Japan

* Corresponding author: nozaki.t.ab@m.titech.ac.jp (Tomohiro Nozaki)

Received: 28 June 2021
Revised: 7 July 2021
Accepted: 9 July 2021
Published online: 12 July 2021

Abstract

Nonthermal plasma-assisted catalysis is shown to be capable of reducing carbon dioxide (CO_2) in the presence of hydrogen (H_2). Dielectric barrier discharge-type plasma-activated CO_2 and H_2 were irradiated on a zinc oxide (ZnO) catalyst, and the surface species and their reaction pathways were investigated via *in situ* transmission infrared absorption spectroscopy. In our previous study on *in situ* Raman spectroscopy of CO_2 hydrogenation on Cu/ZnO, we found the various surface species were uniquely identified on ZnO when DBD was irradiated. Therefore, this study aimed particularly to investigate the effects of nonthermal plasma on support materials (ZnO) without copper. The infrared absorption peaks of the surface species were analyzed via density functional theory (DFT) calculations. Formate (HCOO), formyl group (HCO), and formaldehyde (H_2CO) were generated as reaction products from the plasma and ZnO catalyst. Moreover, the process simultaneously produced plasma-activated hydrogen that adheres to ZnO and undercoordinated Zn in ZnO. These hydrogen adhesions and undercoordinated Zn sites did not appear in thermal reactions in the absence of plasma, suggesting that the plasma-activated hydrogen site in ZnO functions as an active site for the plasma catalytic reaction.

Keywords: CO_2 conversion, carbon recycling, *in situ* spectroscopy, plasma catalysis, nonthermal plasma.

1. Introduction

In order to reduce CO_2 emissions, technological development based on the concept of carbon recycling is being actively promoted [1, 2]. The process of catalytic reduction has been developed to transform CO_2 into valuable resources, such as the production of methanol (CH_3OH). However, this process utilizes high-temperature thermal energy and is not suitable from the viewpoint of carbon recycling because the generation of high-temperature thermal energy is accompanied by combustion, which inevitably produces CO_2 [3].

To reduce environmental impact, renewable energy must be used. Researchers are seeking to develop processes to reduce CO_2 using renewable electricity. Most of these processes are based on electrochemical reactions [4] although various photochemistry and photo-electrochemistry processes that directly use solar energy have recently been reported [5]. As an alternative, the use of plasma generated using renewable power is also being considered. One promising technique is the application of nonthermal plasma–catalyst hybrid processes, also known as plasma catalysis [6, 7]. Plasma catalysis is a process that can transform CO_2 into valuable resources at low temperatures, with plasma-excited CO_2 or hydrogen acting on the catalyst.

Processes that are currently under development as plasma–catalyst hybrid processes [8, 9] include dry reforming under the action of CO_2 and methane (CH_4) [10] and the conversion of CO_2 via direct reduction [11, 12]. The gas can be directly decomposed and utilized in reactions through plasma catalysis. Thus, hydrogen generated through water electrolysis is not used. In addition, the use of plasma is being examined in methanation [13], methanol synthesis [14], and reverse water–gas shift reactions [15], which require hydrogen. The plasma–catalyst hybrid process can be realized at low temperatures. However, the reaction mechanism is

complex. The plasma produces many active species, and the generation path is complicated. Furthermore, the active species react in the gas phase and on solid surfaces.

This study verified the plasma–catalyst hybrid process and analyzed the surface reaction dynamics of CO_2 hydrogenation via an *in situ* transmission Fourier transform infrared (FTIR) spectroscopy system that can perform transmission-type FTIR spectroscopy measurements while simultaneously irradiating a plasma to catalyst. In general, metal catalysts, oxide catalysts, and metal–oxide composite catalysts have been studied for CO_2 hydrogenation to produce CH_3OH. Among these, Cu supported on ZnO (Cu/ZnO) is most widely adapted. Previously, we studied CO_2 hydrogenation on Cu/ZnO by *in situ* Raman spectroscopy under the influence of DBD and found that many different types of surface species was formed on ZnO when DBD was irradiated [16]. Therefore, the purpose of this study was to analyze the surface reaction on support materials ZnO without Cu in plasma irradiation.

In situ analysis can be performed to measure the reaction parameters. *In situ* FTIR spectroscopy [17] was combined with quadrupole mass spectrometry (QMS) [10, 18] to elucidate the reaction mechanism. QMS is advantageous because it quantitatively detects chemical products and the conversion of initial feeds [19]. *In situ* FTIR spectroscopy was performed simultaneously as plasma irradiation. Most of them were diffuse reflectance infrared Fourier transform (DRIFT) [20], and measurements were not performed during plasma irradiation via transmission type FTIR. Compared with DRIFT spectroscopy, transmission infrared (TIR) spectroscopy provides a longer evaluation depth in the sample thickness direction. Thus, the signal strength is stronger and even a small amount of chemical species can be detected. Regarding the production of CH_3OH by CO_2 reduction, HCOO is known as a reaction intermediate. However, the formation of other reaction intermediates in the presence of plasma and the detailed mechanism are unknown.

Plasma was generated using the dielectric barrier discharge (DBD) method [21]. DBD is one of the significant nonthermal plasmas for the following reasons. DBD is a nonequilibrium plasma, and the electron temperature is significantly higher than the gas temperature [22, 23]. Because it is an electronically driven process, a low-power and low-temperature process using renewable energy that does not generate CO_2 will be possible. In addition, DBD is driven at atmospheric pressure [24].

The *in situ* TIR system was applied to evaluate the catalyst surface acting with the $Ar/CO_2/H_2$ plasma. The reaction mechanism on the catalyst surface of active species derived from CO_2 was elucidated. Moreover, the chemical species were analyzed via vibration analysis using density functional theory (DFT) calculations to investigate unstable species and reaction pathways [25, 26].

2. Experimental procedure for i*n situ* TIR spectroscopy under plasma irradiation

ZnO powder (Kanto Chemical Co., Inc.) was compressed at 1.5 MPa, and 1-mm-thick tablets of φ10 mm were obtained. For FTIR (JASCO Corporation: V650) measurements, a mercury–cadmium–telluride (MCT) detector was cooled with liquid nitrogen. The resolution was 4 cm^{-1}, and spectra were accumulated for 1 min and measured over a period of 25 min. Fig. 1 (a) shows the diagrams of the reactor, while Fig. 1(b) presents an image of the plasma emission.

The reaction cell was composed of quartz glass with inner diameter of 25 mm, and zinc selenide (ZnSe) windows were set on both ends of the glass reactor. An electrical heater was attached to the outer side of the reactor to heat the sample. Thermocouples were set near the sample. The heater temperature was set so that the sample temperature became 423 K after the aging was completed, and the experiment was performed. A mixture of Ar, CO_2, and H_2 was introduced via mass flow controllers. The flow rate was set to 100, 60, and 20 cm^3 min^{-1} for Ar, H_2, and CO_2, respectively, at 80 kPa. At this point, background measurements were performed. A DBD type plasma was generated using stainless steel point-to-point (1-mm in diameter) electrodes, where the ground electrode was covered with a quartz sheath. The electrode tip is separated by 10 mm. The catalyst was located at a distance of 5 mm downstream from the DBD. The input peak-to-peak voltage for the DBD was 8–15 kV, with an alternating current frequency of 15 kHz.

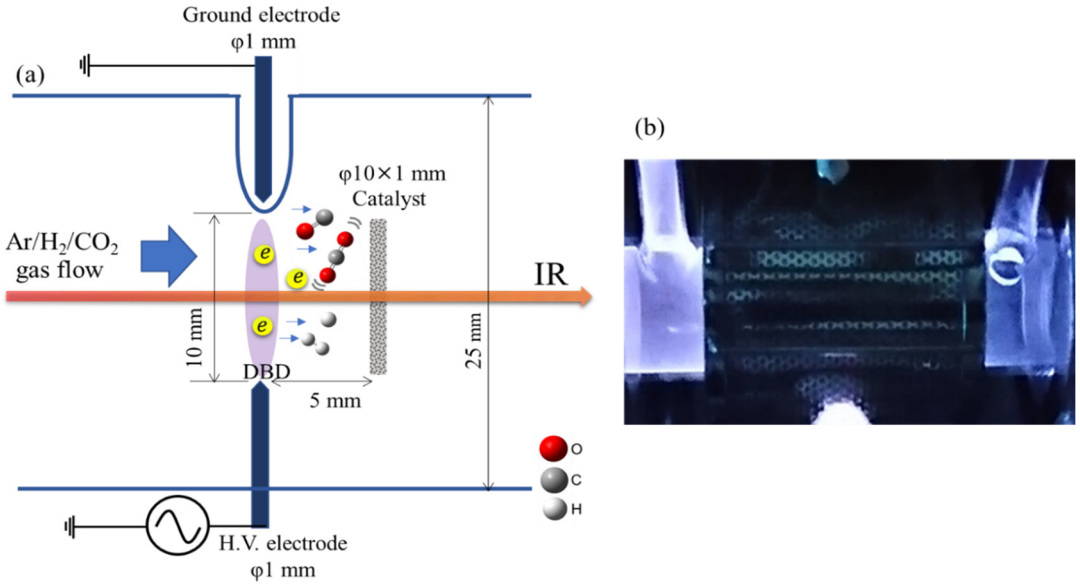

Fig. 1. Schematic of the *in situ* TIR system (a) and an image of plasma emission (b).

3. Results and discussion

3.1 Analysis of ZnO catalyst

A scanning electron microscopy (SEM) (Hitachi High-Tech Corporation: SU8030) image is shown in Fig. 2, while X-ray diffraction (XRD) (Rigaku Corporation: Smart Lab) results of the sample are shown in Fig. 3. These figures show that the ZnO catalyst is hexagonal [27].

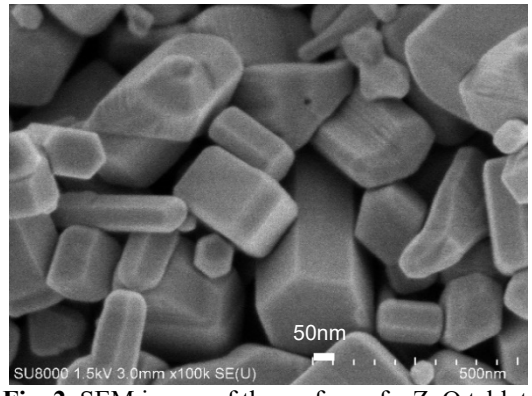

Fig. 2. SEM image of the surface of a ZnO tablet.

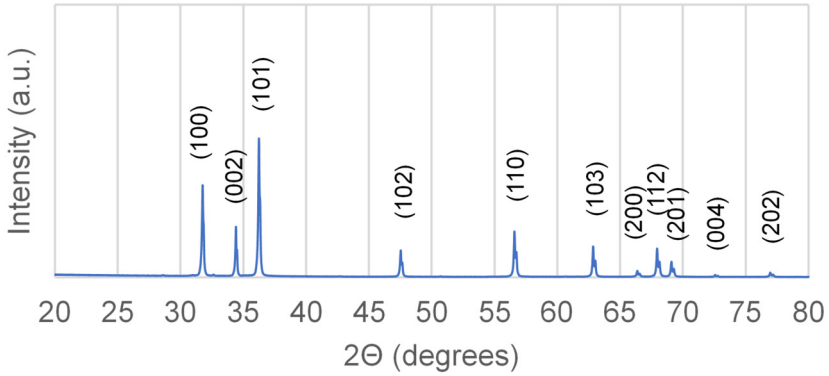

Fig. 3. XRD results for a ZnO tablet.

3.2 *In situ* TIR spectroscopy of plasma-irradiated ZnO

3.2.1 Effects of DBD activated H_2 and CO_2

Figs. 4 show the *in situ* TIR spectra obtained presence Figs. 4 (a), and absence Figs. 4 (b) of plasma. Fig. 4 shows the verification result of the effect of plasma irradiation. In addition, each spectrum was accumulated over a 1-min scan. With the introduction of only Ar and H_2 without plasma, the peaks did not change. However, when the plasma was introduced, new peaks appeared at 670, 685, 750, 800, 952, 1000, 1025, and 1060 cm^{-1}, as shown in Fig. 4 (a). These peaks disappeared in the Ar atmosphere and were present only when the plasma was excited, indicating that the species are highly reactive. Because the peaks appeared to arise from the action of hydrogen-active species, we assumed a structure in which H is bound to ZnO or in which there is a deficiency in ZnO. Of these peaks, the peaks at 952, 1000, 1025, and 1060 cm^{-1} correspond to the adhesion of hydrogen on the generated O caused by the breaking of the Zn–O bond due to Ar and H_2 plasma irradiation, which produces uncoordinated Zn and OH [28]. It behaves as a defect and is considered highly reactive due to the dangling bond. The other peaks at 670, 685, 750, and 800 cm^{-1} have not been previously reported; thus, they were assigned via DFT calculation, as discussed in Section 3.3.

Upon the introduction of CO_2 without plasma, new peaks appeared at 698, 720, and 740 cm^{-1}, as shown in Fig. 4 (b). These peaks appeared in the thermal reaction as well as in the presence of plasma. These peaks cannot be assigned based on previous results in the literature. In addition, these peaks could not be identified via the DFT calculations described in Section 3.3. These peaks behave in the same way as the peak at 2075 cm^{-1} for CO bound to ZnO, as shown in Fig. 5 (a) and (b). Therefore, the vibration of the ZnO lattice to which CO is attached may be the cause of this peak. However, the cause is not clear in this study; thus, further evaluations using another method are required in the future.

As shown in Fig. 4 (a), some peaks appeared in the range of 1300–1700 cm^{-1}, and their intensity increased in the presence of the plasma. The peak at 1425 cm^{-1} was attributed to carbonate [10], while the peaks at 1325, 1371, 1579, and 2878 cm^{-1} were due to HCOO [29, 30]. Spectra for the peak at 2878 cm^{-1} are shown in Supporting Information (1). Other peaks at 1340, 1475, 1512, and 1630 cm^{-1} were assigned via DFT calculations described in Section 3.3, as they have not been previously reported. Because the intensity of these peaks increased even after the plasma was turned off and kept in Ar only, the plasma-activated species reacted with surrounding chemical species after surface adsorption. The increase in these peak intensities under the action of plasma is caused by activated CO_2 produced by vibration excitation. These highly active chemical species are adsorbed and then react on the surface of ZnO.

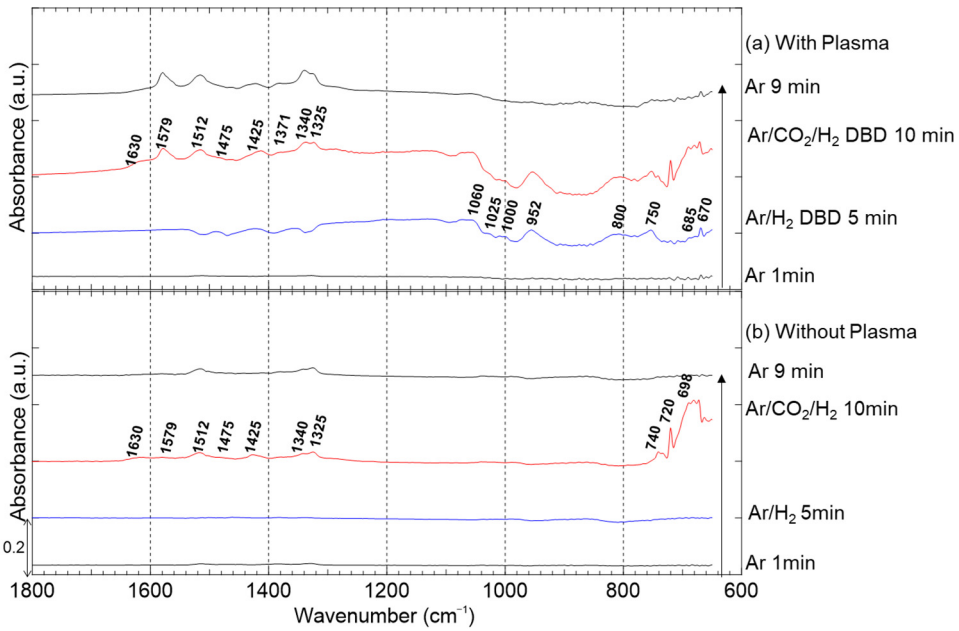

Fig. 4. Comparison of *in situ* TIR spectra under various gas conditions for ZnO. (a) Plasma irradiation, (b) no plasma irradiation (gas flow only). The spectra were acquired during the last minute of processing.

3.2.2 Behavior of CO generated by DBD

Figs. 5 (a) and 5 (b) present enlarged spectra of the CO vibration region in 2000–2250 cm^{-1}. The processing time is shown for each spectrum. The peak at 2075 cm^{-1} appeared in the presence of CO_2 as well, as shown in Fig. 5 (a) and 5 (b), and can be attributed to CO adsorption on ZnO. This peak appeared regardless of the presence of plasma. Thus, it is considered that CO is adsorbed and generated by a catalytic reaction under heat. By contrast, a peak in the range of 2100–2250 cm^{-1} was generated when plasma was available for CO in the gas phase [Fig. 5 (a)] [31, 32]. When 0.3 % CO gas diluted with Ar was introduced on ZnO and measured by *in situ* TIR, gas-phase CO and CO adsorbed onto ZnO were confirmed. This data is not shown. The effect of plasma increases the CO in the gas phase, but the adsorbed CO does not change with or without plasma. Therefore, the plasma-specific peak shown in Fig. 4 (a) in section 3.2.1 is not caused by the adsorption of CO generated by the decomposition of CO_2 to ZnO.

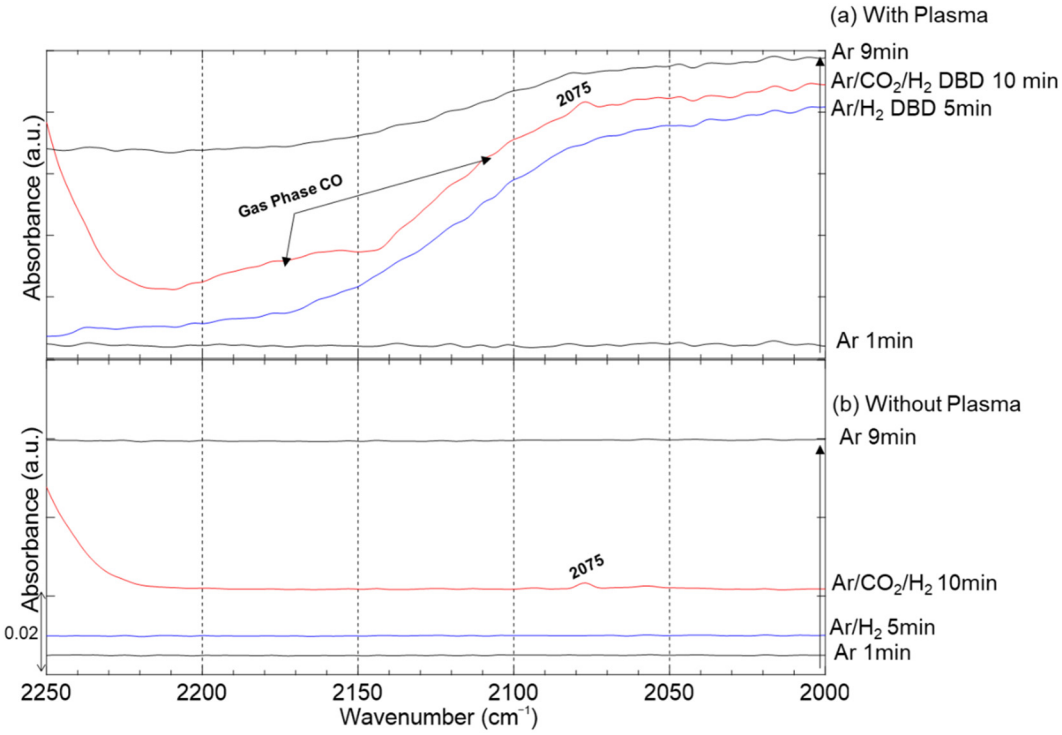

Fig. 5. Comparison of *in situ* TIR spectra for CO vibration region under various gas conditions for ZnO. (a) presents the results obtained with the plasma, while (b) shows the results obtained without the plasma. The spectra were acquired during the last minute of processing.

3.3 DFT analysis

Vibration analysis was performed using a ZnO surface cluster model via DFT. Gas adsorption on the surface of hexagonal ZnO primarily occurs on the (100) surface [33, 34]. Thus, various species were placed on the ZnO (100) surface of the hexagonal crystal construction [35]. As CO_xH_y candidate species, HCOO, HCOOH, HCO, and H_2CO were structurally optimized in ascending order of oxidation number from CO_2, and vibration calculations were performed for those that could be structurally optimized. Fig. 6 shows the optimized structures by DFT calculations. Computational details and further details regarding the cluster model are provided in Supporting Information (2). Vibration analysis was performed after the structural optimization [36]. The calculated wavenumber were scaled by a factor of 0.961, which was proposed for the B3LYP/6–31G(d,p) basis set [37]. Tables 1 and 2 summarize the wavenumber measured via TIR and calculated via DFT, respectively. Table 1 presents the results for the region corresponds to the peak that appears upon irradiation by the Ar/H_2 plasma. Table 2 presents the range corresponding to the vibration of adsorbed species on ZnO by the $Ar/H_2/CO_2$ plasma. As described in Section 3.2, 1325, 1371, 1579, and 2878 cm^{-1} can be attributed to HCOO [29, 30] according to the literature, fitting well with this DFT calculation.

We examined the experimental peaks at 685, 750, and 800 cm^{-1}, which appeared under Ar/H_2 plasma activation and could not be assigned in Section 3.2.1, as shown in Table 1. Similarly, the peak at 750 cm^{-1} was attributed to the motion of H coupled with the O in ZnO. The peak of DFT calculation corresponding to this peak is 723 cm^{-1}. The peaks at 685 and 800 cm^{-1}, which were calculated as 717 and 816 cm^{-1}, respectively, correspond to OH motion on ZnO.

Next, we assigned the peaks at 1340, 1475, 1512, 1630, and 2978 cm^{-1}, which were generated by $Ar/H_2/CO_2$ plasma activation. The *in situ* TIR spectra including the peak at 2978 cm^{-1} for the range of 2600–3200 cm^{-1} is described in Supporting Information (1). As shown in Table 2, the peaks at 1340 and 1512 cm^{-1} were attributed to HCO vibrations which correspond to the 1347 and 1569 cm^{-1}. Furthermore, the peaks at 1475 and 1630 cm^{-1} were attributed to H_2CO vibrations which correspond to 1453 and 1680 cm^{-1}. The DFT peaks corresponding to 2970 and 2982 cm^{-1} for HCO and H_2CO are close and, therefore, a single experimental peak at 2978 cm^{-1} could not be assigned to the HCO and/or H_2CO peaks.

Table 1. DFT-calculated and experimental TIR wavenumber (cm^{-1}) of infrared active vibrational modes for H and OH on ZnO.

	(a) OH		(b) (O)-H	
	DFT	TIR	DFT	TIR
H−O bending (out-of-plane)	717	685	723	750
H−O bending (in-plane)	816	800		
H−O stretching	3619		3659	

Table 2. DFT-calculated and experimental TIR wavenumber (cm^{-1}) of infrared active vibrational modes for H_2CO, HCO, and HCOO on ZnO.

	(c) H_2CO		(d) HCO		(e) HCOO	
	DFT	TIR	DFT	TIR	DFT	TIR
O–C–O bending (in-plane, sym.)			734		726	
H–C bending (out-of-plane)			1030		1025	
H–C–H bending (out-of-plane, sym.)	1201					
H–C–O bending (in-plane, asym.)	1242					
C–O stretching O–C–O stretching (sym.)			1275		1336	1325
H–C–O bending (in-plane, asym.)			1347	1340	1372	1371
H–C–H bending (in-plane, sym.)	1453	1475				
O–C–O stretching (asym.)			1569	1512	1585	1579
O–C stretching + H–C–O bending (in-plane, sym.)	1680	1630				
H–C–H stretching (sym.)	2862					
H–C stretching			2970	2978*	2916	2878
H–C–H stretching (asym.)	2982	2978*				

"*" corresponds to the wavenumber of 2978 cm^{-1}, which is listed for both H_2CO and HCO because these peaks cannot be distinguished using the experimental results.

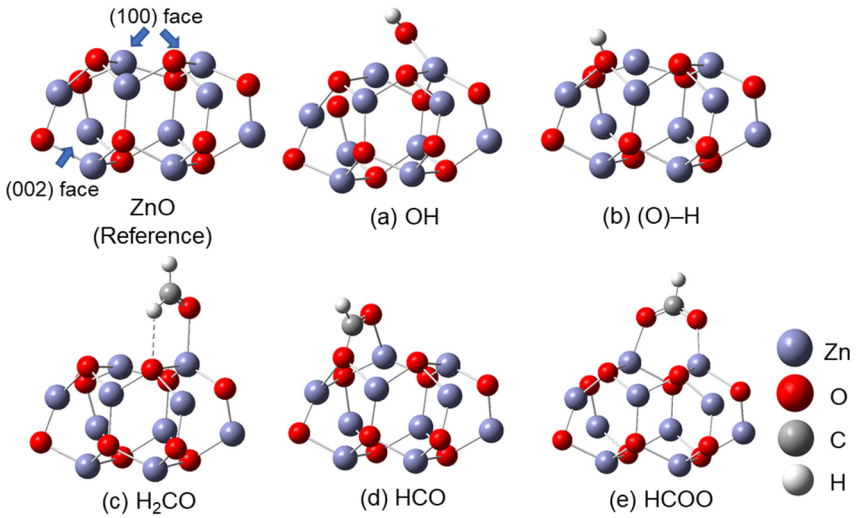

Fig. 6. Geometries optimized via DFT calculations at the B3LYP/6-31G(d,p) level.

3.4 Reaction mechanisms

Cu/ZnO is studied in CO_2 hydrogenation to CH_3OH. Previously, we studied Cu/ZnO using *in situ* Raman spectroscopy [16]. We found that various surface species are formed rather selectively on ZnO and few species were identified on Cu. Therefore, in this study, we focused on the detailed analysis of ZnO surface by *in situ* TIR during plasma irradiation. Because Cu is absent in this study, CH_3OH was not synthesized; however, the reaction behavior of HCOO, as CH_3OH precursor, is discussed in detail [38]. The species adsorbed onto the surface of ZnO are indicated by "*", and the species in the vibrationally excited state are indicated by "^{V}". H_2 are adsorbed onto the surface of ZnO and decomposed into H (R1). The reaction itself occurs with or without plasma [39]. However, as a reaction peculiar to plasma, the surface was changed by the effect of plasma and dangling bonds are generated. The adsorption of H_2 is promoted, and as a result, the decomposition into H is promoted (R2). The electrons collided with CO_2 to generate CO_2^V (R3) or CO (R5) in plasma [11, 40]. CO_2^V combines with oxygen anion sites (O^{2-}) on the surface of ZnO to form CO_3^{2-*} (R4) [38]. Meanwhile, CO forms a carbonyl bond with the ZnO surface (R6) [41]. H* and CO_3^{2-*} form HCOO* (R7) [20]. Similarly, x H* and CO* form H_xCO* (x = 1, 2) (R8), while CO_2^V reacts with H* to form HCOO (R9) [42].

HCOO* reacts with H* to produce HCO* (R10), and HCO* reacts with H* to produce H_2CO* (R11) [38]. Because CO_3^{2-*} is generated (R4), the possibility of the Langmuir–Hinshelwood (L–H) mechanism due to H* on the surface of ZnO is considered for the generation of HCOO* (R7) [20].

Regarding the reaction between CO* and H* (R8), it can be seen that the CO* reaction is not plasma-specific as CO* is generated even in the absence of plasma [Fig. 5 (a), (b)]. Therefore, the effect of this reaction is considered to be very small. (R7), (R9), (R10), and (R11) benefit from plasma because plasma promotes the production of H* and CO_3^{2-}.

The Eley–Rideal (E–R) mechanism is also considered for H* and CO_2^V in producing HCOO* (R9) [34]. In plasma, CO species can arise from electron excitation (R5) and CO_2^V due to vibration excitation (R3) [40]. It is known that the vibration energy of CO_2^V is important for generating HCOO (R9) [42].

In addition, the intensity of *in situ* TIR spectra for HCOO*, HCO*, and H_2CO* increased approximately 1.2-fold in the Ar atmosphere after plasma irradiation. Moreover, the intensity of CO_3^{2-*} decreased by 25% (R7), and H* disappeared (R7, R10, R11). This result supports the L–H mechanism rather than the rapid E–R mechanism.

$$H_2 \rightarrow H_2^* \quad \text{(R1)}$$

$$H_2^* \rightarrow H^* + H^* \quad \text{(R2)}$$

$$CO_2 + e \rightarrow CO_2^v + e \quad \text{(R3)}$$

$$CO_2^{v} + O^{2-}* \rightarrow CO_3^{2-}* \quad \text{(R4)}$$

$$CO_2 + e \rightarrow CO + O + e \quad \text{(R5)}$$

$$CO \rightarrow CO* \quad \text{(R6)}$$

$$CO_3^{2-}* + H* \rightarrow HCOO* + O^{2-}* \quad \text{(R7)}$$

$$CO* + x\,H* \rightarrow H_xCO* \ (x = 1, 2) \quad \text{(R8)}$$

$$CO_2^{v} + H* \rightarrow HCOO* \quad \text{(R9)}$$

$$HCOO* + H* \rightarrow HCO* + OH* \quad \text{(R10)}$$

$$HCO* + H* \rightarrow H_2CO* \quad \text{(R11)}$$

The lifetime of active species can be discussed from the timescale of reactions in plasma, which is summarized by Kim *et al* shown in Fig.7 [43]. Lifetime of radicals are estimated to be 10^{-7} s. On the other hand, in the vibrationally excited state, the lifetime is approximately 10^{-5} to 10^{-3} s. Therefore, vibrationally excited CO_2 would contribute more to the surface reaction than radicals. The vibrationally excited states is discussed not only for CO_2 but also for H_2 [44].

Energy distribution to each excited state was analyzed numerically in various CO_2 plasma [45]. Generally, microwave plasma generates low-energy electron plasma which is more favored to produce vibrationally excited CO_2 than DBD. Meantime, the discharge property of DBD is modified by operating frequency, generating more vibrationally excited species at higher frequency (e.g. 100 kHz) [10]. Therefore, DBD can tune the production rate of radical and vibrational species. However, selective production of desired species by plasma alone is not possible: therefore, to enhance the reaction selectivity, we propose the combination of heterogeneous catalysts and DBD. Based on the reaction mechanism clarified in this study, we would be able to pursue a better catalyst for plasma catalysis, enabling low-temperature CO_2 hydrogenation to CH_3OH at a high yield.

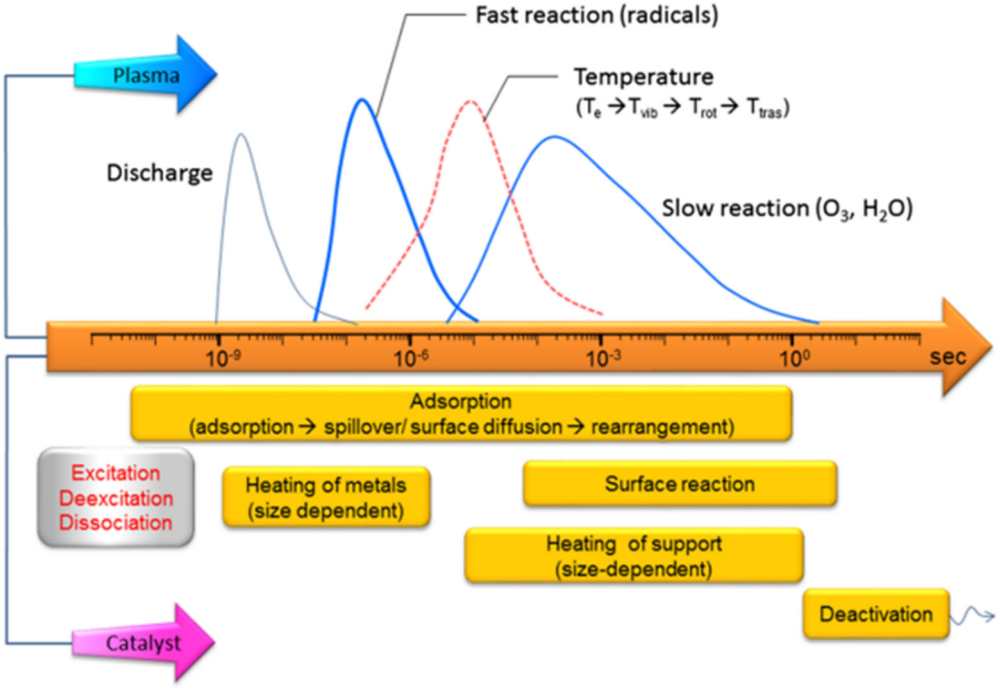

Fig. 7. The time-scales in plasma and catalytic reaction (reproduced from ref. [43] with permission from the pulisher).

4. Conclusion

In this study, the plasma–catalyst hybrid process was verified, and the surface product and reaction path of the ZnO catalyst acting on plasma activated CO_2 and H_2 at 423 K were clarified via *in situ* TIR and DFT calculations. Active sites formed in ZnO due to the active hydrogen species in the Ar/H_2 plasma. These sites correspond to H adsorbed on the O of ZnO. In addition, uncoordinated Zn also formed. These sites are too reactive to be detected without using this specialized technique of *in situ* TIR system. In the presence of activated $Ar/H_2/CO_2$ plasma, HCOO, HCO, H_2CO, and CO_3^{2-} were produced. In the reaction path, CO did not contribute to the reaction, while the vibration excitation of CO_2 provided a substantial contribution. Therefore, when applying the plasma–catalyst hybrid process for CO_2 reduction of valuable compounds on ZnO, the vibrational excitation of CO_2 and the formation of active sites by plasma-activated hydrogen are important. These results are essential information for catalyst design where hydrogen adsorption points are incorporated on the catalyst surface. In addition, these are very important as the guidelines for setting the conditions of the plasma catalyst process in terms of generating H adsorption points by plasma and the control of vibrationally excited CO_2. This study is a new effort to analyze the reaction mechanism by *in situ* TIR during plasma irradiation. In the future, further details can be understood by considering it in combination with quantitative consideration by QMS.

Acknowledgements

This project was supported by the JST CREST (JPMJCR19R3). Z. S. acknowledges the financial support from the China Scholarships Council program (201707040056).

References

[1] Quadrelli E. A., Centi G., Duplan J-L., and Perathoner S., Carbon dioxide recycling: Emerging large-scale technologies with industrial potential, *ChemSusChem*, Vol. 4 (9), pp. 1194–1215, 2011.
[2] He M., Sun Y., and Han B., Green carbon science: Scientific basis for integrating carbon resource processing, utilization, and recycling, *Angew. Chem. Int. Ed*., Vol. 52 (37), pp. 9620–9633, 2013.
[3] Centi, G. and Perathoner, S., Opportunities and prospects in the chemical recycling of carbon dioxide to fuels, *Catal. Today*, Vol. 148 (3–4), pp. 191–205, 2009.
[4] Le, M., Ren, M., Zhang, Z., Sprunger, P. T., Kurtz, R. L., and Flake, J. C., Electrochemical Reduction of CO_2 to CH_3OH at Copper Oxide Surfaces, *J. Electrochem. Soc*., Vol. 158 (5), p. E45, 2011.
[5] Wang, W. H., Himeda, Y. J. T., Muckerman, G. F. Manbeck, and Fujita, E., CO_2 Hydrogenation to formate and methanol as an alternative to photo- and electrochemical CO_2 reduction, *Chem. Rev*., Vol. 115 (23), pp. 12936–12973, 2015.
[6] Bogaerts, A., Tu X., Whitehead J. C., Centi G., Lefferts L., Guaitella O., Azzolina-Jury F., Kim H. H., Murphy A. B., Schneider W. F., Nozaki T., Hicks J. C., Rousseau A., Thevenet F., Khacef A., and Carreon M., The 2020 plasma catalysis roadmap, *J. Phys. D. Appl. Phys*., Vol. 53 (44), pp. 443001, 2020.
[7] Kim, H.H., Abdelaziz, A. A., Teramoto, Y., Nozaki, T. and Hensel, K., Mok, Y.S., Saud S., Nguyen D.B., Lee, D.H., and Kang W.S., Interim report of plasma catalysis: Footprints in the past and blueprints for the future, *Int. J. Plasma Environ. Sci. Technol*., Vol. 15 (1), pp. e01004, 2021.
[8] Whitehead, J. C., Plasma-catalysis: Is it just a question of scale?, *Front. Chem. Sci. Eng*., Vol. 13 (2), pp. 264–273, 2019.
[9] Mehta, P., Barboun, P., Go, D. B., Hicks, J. C., and Schneider, W. F., Catalysis enabled by plasma activation of strong chemical bonds: A Review, *ACS Energy Lett*., Vol. 4 (5), pp. 1115–1133, 2019.
[10] Sheng, Z., Watanabe, Y., Kim, H. H., Yao, S., and Nozaki, T., Plasma-enabled mode-selective activation of CH_4 for dry reforming: First touch on the kinetic analysis, *Chem. Eng. J*., Vol. 399, pp. 125751, 2020.
[11] Adrianto, D., Sheng, Z., and Nozaki, T., Mechanistic study on nonthermal plasma conversion of CO_2, *Int. J. Plasma Environ. Sci. Technol*., Vol. 14 (1), pp. e01003, 2020.
[12] Mei, D., Zhu, X., Wu, C., Ashford, B., Williams, P. T., and Tu, X., Plasma-photocatalytic conversion of CO_2 at low temperatures: Understanding the synergistic effect of plasma-catalysis, *Appl. Catal. B Environ*., Vol. 182, pp. 525–532, 2016.
[13] Kano, M., Satoh, G., and Iizuka, S., Reforming of carbon dioxide to methane and methanol by electric impulse low-pressure discharge with hydrogen, *Plasma Chem. Plasma Process*., Vol. 32 (2), pp. 177–185, 2012.
[14] Wang, L., Yi, Y., Guo, H., and Tu, X., Atmospheric Pressure and Room Temperature Synthesis of Methanol

through Plasma-Catalytic Hydrogenation of CO_2, *ACS Catal*., Vol. 8 (1), pp. 90–100, 2018.
[15] Liu L., Das S., Chen T., Dewangan N., Ashok J., Xi S., Borgna A., Li Z., and Kawi S., Low temperature catalytic reverse water-gas shift reaction over perovskite catalysts in DBD plasma, *Appl. Catal. B Environ*., Vol. 265, pp. 118573, 2020.
[16] Saito, A., Sheng, Z., and Nozaki, T., *In situ* Raman spectroscopy of plasma – catalyst interface for conversion of CO_2 and CH_4 to valuable compounds, *Int. J. Plasma Environ. Sci. Technol*., Vol. 15, pp. e02007, 2021.
[17] Adarsh, K. S., Chandrasekaran, N., and Chakrapani, V., *In-situ* spectroscopic techniques as critical evaluation tools for electrochemical carbon dioxide reduction: A mini review, *Front. Chem*., Vol. 8, pp. 1–9, 2020.
[18] Lu., H., Yao X., Li J., Yao S., Wu Z., Zhang H., Lin H., and Nozaki T., Mechanism on the plasma-catalytic oxidation of graphitic carbon over Au/γ-Al_2O_3 by *in situ* plasma DRIFTS-mass spectrometer, *J. Hazard. Mater*., Vol. 396, pp. 122730, 2020.
[19] Sheng. Z., Sakata, K., Watanabe., Y., Kameshima., S. Kim., H. H., Yao., S., Nozaki., T., Factors determining synergism in plasma catalysis of biogas at reduced pressure, *J. Phys. D. Appl. Phys*., Vol. 52 (41), pp. 414002, 2019.
[20] Sheng, Z., Kim, H. H., Yao, S., and Nozaki, T., Plasma-chemical promotion of catalysis for CH_4 dry reforming: Unveiling plasma-enabled reaction mechanisms, *Phys. Chem. Chem. Phys*., Vol. 22 (34), pp. 19349–19358, 2020.
[21] Li, J., Ma, C., Zhu, S., Yu, F., Dai, B., and Yang, D., A review of recent advances of dielectric barrier discharge plasma in catalysis, *Nanomaterials*, Vol. 9 (10), pp. 1–34, 2019.
[22] Nozaki, T., Miyazaki, Y., Unno, Y., and Okazaki, K., Energy distribution and heat transfer mechanisms in atmospheric pressure non-equilibrium plasmas, *J. Phys. D. Appl. Phys*., Vol. 34 (23), pp. 3383–3390, 2001.
[23] Chen, H., Mu, Y., Xu, S., Xu S., Hardacre, C., and Fan, X., Recent advances in non-thermal plasma (NTP) catalysis towards C1 chemistry, *Chinese J. Chem. Eng*., Vol. 28 (8), pp. 2010–2021, 2020.
[24] Kogelschatz, U., Dielectric-barrier discharges: Their history, discharge physics, and industrial applications, *Plasma Chem. Plasma Process*., Vol. 23 (1), pp. 1–46, 2003.
[25] Li, X., and Paier, J., Vibrational properties of CO_2 adsorbed on the Fe_3O_4 (111) surface: Insights gained from DFT, *J. Chem. Phys.*, Vol. 152 (10), pp. 104702, 2020.
[26] Kucharska, E., Hanuza, J., Ciupa, A., Mączka, M., and Macalik, L., Vibrational properties and DFT calculations of formamidine-templated Co and Fe formates, *Vib. Spectrosc*., Vol. 75, pp. 45–50, 2014.
[27] Raza, W., Faisal, S. M., Owais, M., Bahnemann, D., and Muneer, M., Facile fabrication of highly efficient modified ZnO photocatalyst with enhanced photocatalytic, antibacterial and anticancer activity, *RSC Adv*., Vol. 6 (82), pp. 78335–78350, 2016.
[28] Wardle, M. G., Goss, J. P., and Briddon, P. R., Theory of Fe, Co, Ni, Cu, and their complexes with hydrogen in ZnO, *Phys. Rev. B - Condens. Matter Mater. Phys*., Vol. 72 (15), pp. 155108, 2005.
[29] Nakamura, J., Choi, Y., and Fujitani, T., On the issue of the active site and the role of ZnO in Cu/ZnO methanol synthesis catalysts, *Top. Catal*., Vol. 22 (3–4), pp. 277–285, 2003.
[30] Andrews, E., Ren, M., Wang, F., Zhang, Z., Sprunger, P., Kurtz, R., and Flake, J., Electrochemical reduction of CO_2 at Cu nanocluster / (10$\bar{1}$0) ZnO Electrodes, *J. Electrochem. Soc*., Vol. 160 (11), pp. H841–H846, 2013.
[31] Abdel-Mageed, A. M., Klyushin, A., Rezvani, A., Knop-Gericke, A., Schlögl, R., and Behm, R. J., Negative charging of Au nanoparticles during methanol synthesis from CO_2/H_2 on a Au/ZnO catalyst: Insights from operando IR and near-ambient-pressure XPS and XAS measurements, *Angew. Chemie - Int. Ed*., Vol. 58 (30), pp. 10325–10329, 2019.
[32] Schumann, J., Kröhnert, J., Frei, E., Schlögl, R., and Trunschke, A., IR-spectroscopic study on the interface of Cu-based methanol synthesis catalysts: Evidence for the formation of a ZnO overlayer, *Top. Catal*., Vol. 60 (19–20), pp. 1735–1743, 2017.
[33] Shi, H., Yuan, H., Ruan, S.,Wang, W., Li, Z., Li, Z., Shao, X., Adsorption and diffusion of CO on clean and CO_2-precovered ZnO (10$\bar{1}$0), *J. Phys. Chem. C*, Vol. 122 (16), pp. 8919–8924, 2018.
[34] Li, Z., Yuan, H., Sun, Y., Zhang, J., Li, Z., and Shao, X., Dissociative adsorption and linear organization of formic acid on ZnO(1 0 −1 0) surface, *J. Catal*., Vol. 390, pp. 109–116, 2020.
[35] Lintuluoto, M., Nakatsuji, H., Hada, M., and Kanai, H., Theoretical study of the decomposition of HCOOH on an MgO(100) surface, *Surf. Sci*., Vol. 429 (1), pp. 133–142, 1999.
[36] Mino, L., Spoto, G., and Ferrari, A. M., CO_2 capture by TiO_2 anatase surfaces: A combined DFT and FTIR study, *J. Phys. Chem. C*, Vol. 118, no. 43 (43), pp. 25016–25026, 2014.
[37] Irikura, K. K., Johnson, R. D., and Kacker, R. N., Uncertainties in scaling factors for ab initio vibrational frequencies, *J. Phys. Chem. A*, Vol. 109 (37), pp. 8430–8437, 2005.
[38] Yang, R., Zhang, Y., and Tsubaki, N., Rideal-type reaction of formate species with alcohol: A key step in new low-temperature methanol synthesis method, *Catal. Commun*., Vol. 8 (11), pp. 1829–1833, 2007.
[39] Lü, X., Xu, X., Wang, N., Zhang, Q., Ehara, M., and Nakatsuji, H., Heterolytic adsorption of H_2 on ZnO(10$\bar{1}$0) surface: An ab initio SPC cluster model study, *J. Phys. Chem. B*, Vol. 103 (14), pp. 2689–2695, 1999.
[40] Pietanza, L. D., Colonna, G., D'Ammando, G., Laricchiuta, A., and Capitelli, M., Electron energy distribution functions and fractional power transfer in 'cold' and excited CO_2 discharge and post discharge conditions, *Phys. Plasmas*, Vol. 23 (1), 2016.

[41] Boccuzzi, F. and Chiorino, A., FTIR study of carbon monoxide oxidation and scrambling at room temperature over copper supported on ZnO and TiO_2. 1, *J. Phys. Chem*., Vol. 100 (9), pp. 3617–3624, 1996.
[42] Quan, J., Muttaqien F., Kondo T., Kozarashi T., Mogi T., Imabayashi T., Hamamoto Y., Inagaki K., Hamada I., Morikawa Y., and Nakamura J., Vibration-driven reaction of CO_2 on Cu surfaces via Eley–Rideal-type mechanism, *Nat. Chem*., Vol. 11 (8), pp. 722–729, 2019.
[43] Kim, H. H., Teramoto, Y., Ogata, A., Takagi, H., and Nanba, T., Plasma Catalysis for Environmental Treatment and Energy Applications, *Plasma Chem. Plasma Process*., Vol. 36 (1), pp. 45–72, 2016.
[44] Hong, J., Pancheshnyi, S., Tam, E., Lowke, J.J., Prawer, S., and Murphy, A. B., Kinetic modelling of NH_3 production in N_2-H_2 non-equilibrium atmospheric-pressure plasma catalysis, *J. Phys. D. Appl. Phys*., Vol. 50 (15), pp. 154005, 2017.
[45] Bogaerts, A., Kozák, T., Van Laer, K., and Snoeckx, R., Plasma-based conversion of CO_2: Current status and future challenges, *Faraday Discuss*., Vol. 183, pp. 217–232, 2015.

Supporting Information

S1. Peaks at 2878 and 2978 cm^{-1} were generated by $Ar/CO_2/H_2$ plasma irradiation on ZnO

The peaks of 2878 and 2978 cm^{-1} were slightly generated during plasma irradiation. They increased during retention in the Ar atmosphere after plasma irradiation. This indicates that a slow surface reaction occurs, and we considered it the Langmuir–Hinshelwood (L-H) mechanism.

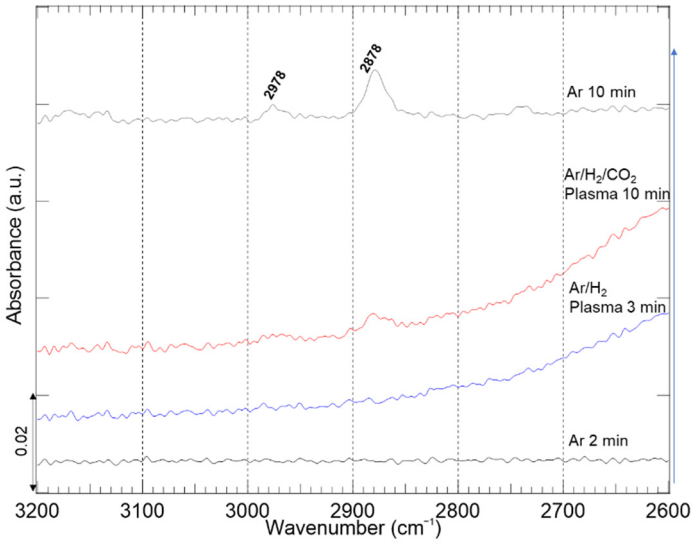

Fig. S1. *In situ* TIR spectra obtained for plasma irradiation of a ZnO tablet. The spectra were acquired during the last minute of processing.

S2. Computational Details

Our experiment showed that the (100) surface of hexagonal ZnO was exposed; thus, a two-layer model of the (100) surface of hexagonal ZnO was built. The initial geometrical parameters of the (100) ZnO surface model [s1] were taken from the X-ray structure shown in Fig. 3. Chemical species were placed on the first layer of the ZnO surface model. The second layer was fixed, and the chemical species and first layer were fully relaxed. The second layer of ZnO is calculated by fixing the coordinates of the stable structure of ZnO alone. If the structure of ZnO adsorbing functional groups is optimized without fixing the second layer, the hexagonal crystals of ZnO are not maintained.The active species were placed on Zn and O, and at an intermediate position between Zn and O, and the calculation was started, and the structure-optimized structures with low energy were subjected to vibration analysis. Although an imaginary wavenumber appeared for the chemical species in Fig. 6 (a), (b), (d), and (e), they primarily originated from the second layer of ZnO, not the first layer, indicating that the vibration analysis is less affected by the imaginary wavenumber. All calculations were performed at the B3LYP [s2]/ 6-31G(d,p) [s3] level by Gaussian16 [s4]. Since the vibration intensity is sensitive to the cluster model situation, especially the symmetry. it is not discussed this study [s5, s6].

References

[s1] Bououdina, M., Azzaza, S., Ghomri, R., Shaikh, M. N., Dai, J. H., Song, Y., Song, W., Cai, W., and Ghers, M., Structural and magnetic properties and DFT analysis of ZnO:(Al,Er) nanoparticles, *RSC Adv.*, Vol. 7, pp. 32931–32941, 2017.

[s2] Stephen, P. J., Devlin, F. J., Chabalowski, C. F., and Frisch, M. J., Ab Initio Calculation of Vibrational Absorption, *J. Phys. Chem.*, Vol. 98, 11623–11627, 1994.

[s3] https://www.basissetexchange.org/

[s4] Gaussian 16, Revision C.01, Frisch, M. J.; Trucks, G. W.; Schlegel, H. B.; Scuseria, G. E.; Robb, M. A.; Cheeseman, J. R.; Scalmani, G.; Barone, V.; Petersson, G. A.; Nakatsuji, H.; Li, X.; Caricato, M.; Marenich, A. V.; Bloino, J.;

Janesko, B. G.; Gomperts, R.; Mennucci, B.; Hratchian, H. P.; Ortiz, J. V.; Izmaylov, A. F.; Sonnenberg, J. L.; Williams-Young, D.; Ding, F.; Lipparini, F.; Egidi, F.; Goings, J.; Peng, B.; Petrone, A.; Henderson, T.; Ranasinghe, D.; Zakrzewski, V. G.; Gao, J.; Rega, N.; Zheng, G.; Liang, W.; Hada, M.; Ehara, M.; Toyota, K.; Fukuda, R.; Hasegawa, J.; Ishida, M.; Nakajima, T.; Honda, Y.; Kitao, O.; Nakai, H.; Vreven, T.; Throssell, K.; Montgomery, J. A., Jr.; Peralta, J. E.; Ogliaro, F.; Bearpark, M. J.; Heyd, J. J.; Brothers, E. N.; Kudin, K. N.; Staroverov, V. N.; Keith, T. A.; Kobayashi, R.; Normand, J.; Raghavachari, K.; Rendell, A. P.; Burant, J. C.; Iyengar, S. S.; Tomasi, J.; Cossi, M.; Millam, J. M.; Klene, M.; Adamo, C.; Cammi, R.; Ochterski, J. W.; Martin, R. L.; Morokuma, K.; Farkas, O.; Foresman, J. B.; Fox, D. J. Gaussian, Inc., Wallingford CT, 2016.

[s5] Yi Li, Yuanyuan Liu, Haowei Wang, Xiaohui Xiong, Ping Wei, and Fangshi, Synthesis, Crystal Structure, Vibration Spectral, and DFT Studies of 4-Aminoantipyrine and Its Derivatives, *Molecules*, Vol. 18, pp. 877-893, 2013.

[s6] Breedon, M., Spencer, M.J.S., Yarovsky, I., Adsorption of NO and NO_2 on the ZnO(2 -1 -1 0) surface: A DFT study, *Surface Sci.*, Vol. 603, pp. 3389–3399, 2009.)